Direct Determination of Intermolecular Structure of Ethanol Adsorbed in Micropores using X-ray Diffraction and Reverse Monte Carlo Analysis

Taku Iiyama*, Kousuke Hagi, Takafumi Urushibara, and Sumio Ozeki

Department of Chemistry, Faculty of Science, Shinshu University, 3-1-1 Asahi, Matsumoto, Nagano 390-8621, Japan

tiiyama@shinshu-u.ac.jp

keywords: intermolecular structure, XRD, adsorption, activated carbon fiber, radial distribution function

Abstract

The intermolecular structure of C_2H_5OH molecules confined in slit-shaped graphitic micropore of activated carbon fiber was investigated by *in situ* X-ray diffraction (XRD) measurement and reverse Monte Carlo (RMC) analysis. The pseudo-3-dimensional intermolecular structure of C_2H_5OH adsorbed in the micropores was determined by applying the RMC analysis to XRD data, assuming a simple slit-shaped space composed of double graphene sheets. The results were consistent with conventional Monte Carlo simulation; e.g., bilayer structure formed by hydrogen bonds among C_2H_5OH adsorbed at low fractional filling. The RMC method based on experimental XRD data may be a useful tool to estimate the 3-dimensional structure of adsorbed phase confined in pores.

1. Introduction

The direct determination method for intermolecular structures of a condensed phase in limited spaces has been strongly desired from the viewpoint of catalytic, biological,

and adsorption science. Recently, importance of porous materials is increasing in energy and environmental fields, for example, the safe storage of supercritical gases such as methane and hydrogen and the removal of toxic substances from emission gases and tap water. Molecules are caught in micropore by enhanced interaction between surface and admolecules, which arises from overlapped potential due to both walls [1]. Furthermore, since the molecular number in an adsorption phase is extremely small in comparison with a bulk phase [2], many unique phenomena may occur in the pore even at ambient temperature and moderate pressure. Therefore, a direct approach to the intermolecular structure between molecules adsorbed in micropores is helpful in understanding adsorption processes and molecular behavior in the limited spaces. The approach can give an essential information for the design of new porous materials.

The direct method detecting molecular assemblies in pores is very limited, because the pore is a space surrounded by a solid. As X-rays can penetrate various materials, one can detect directly the structural information of molecular assemblies in pores. We used X-ray diffraction (XRD) and small angle X-ray scattering (SAXS) techniques in order to elucidate the intermolecular and assembly structure in micropores. The radial distribution function (RDF) of water adsorbed in carbon micropores was determined by *in situ* XRD measurements. The analysis showed that the water phase was solid-like even at room temperature [3, 4]. In the case of CCl_4 in carbon micropores, CCl_4 molecules lost the long-range order owing to spatial restriction [5,6]. The density fluctuation and correlation length of water adsorbed on activated carbons estimated from SAXS gave evidence of the formation of cluster-like assemblies in micropores [2, 7]. Water was adsorbed in carbon micropores in spite of hydrophobic surfaces, when clusters of more than 0.4 nm in radius were formed [2]. The cluster size corresponds to an assembly of about 12 water molecules. It seems that the property of the water should be changed from hydrophilicity to hydrophobicity by clustering in carbon micropores [8]. Recently, the precise position analyses of admolecules in porous crystals were carried out by XRD measurement and Rietvelt analysis [9,10]. The investigation of the local structure around a metal ion in pores was also carried out with EXAFS [11].

Computer simulation is a suitable method to obtain intermolecular structure of adsorbates in pores, since the number of molecule in the system is generally small. Therefore, the method has been frequently used to investigate physical adsorption [12–

16], such as water adsorption on hydrophobic surfaces [17–19].

Two assumptions may be required in order to apply the computer simulation to an adsorption system. One is the shape of a pore, another is the potentials between admolecules and between an admolecule and surface. In general, a simplified pore with periodic boundaries is used as a simulation cell and the potential function between molecules is used, that is sufficiently verified in a bulk state. The experimental values to clarify results of the simulation seem to be limited to adsorption amount and heat of adsorption.

On the other hand, it is possible to obtain RDF from *in situ* XRD results without any assumption. However, RDF is 1-dimensional structural information that is averaged over all molecules in the whole system. We applied reverse Monte Carlo (RMC) method to an adsorption system in order to obtain the 3-dimensional structure of an adsorbed phase. There are no application of the RMC method to adsorption phase, although RMC methods [20] have been used in order to estimate intermolecular structure of disordered materials such as glasses, amorphous materials [21,22], and liquids [23–25] from their experimental structural information. We here tried to determine the structure of molecules adsorbed in micropores by combination of XRD data and RMC analysis.

Since C_2H_5OH is amphiphilic, the intermolecular structure of C_2H_5OH molecules interacting with hydrophobic surfaces is quite interesting from the viewpoint of competitive formation of hydrogen bonds and hydrophobic bonds. Morishige et. al. concluded by XRD analysis that C_2H_5OH molecules on graphite surfaces formed a 2-dimensional crystal structure with zigzag hydrogen bond chains at low temperature [26]. In carbon micropores, the RDF analysis showed that C_2H_5OH formed an ordered structure even at ambient temperature [27]. Recently, we reported preliminary results of the RMC simulation for water adsorbed in micropores of an activated carbon fiber [28]. In this paper, we here propose the RMC simulation for adsorption systems: a pseudo-3-dimensional structure of C_2H_5OH adsorbed in graphitic slit-shaped micropores has been constructed by combination of XRD data and RMC analysis.

2. Experimental Section

A pitch-based activated carbon fiber, ACF (A10; Ad'all Co., Ltd.), was used as an adsorbent. The micropore structure was determined from an N_2 adsorption isotherm with a gravimetric method at 77 K after pre-heating at 383 K and 1 mPa for 2 h. Adsorption isotherms of C_2H_5OH was determined by a volumetric method at 300 K after pre-treatment similar to N_2 adsorption.

The XRD of C_2H_5OH adsorbed on A10 was measured by a transmission method with a Rigaku angle-dispersion diffractometer (MultiFlex) in the scattering angle 2θ = 5 – 105° (s = 3.6 – 64.6 nm^{-1}). The monochromatic CuKα radiation (λ = 0.15418 nm) was generated from the X-ray tube operated at 40 kV and 20 mA. The sample chamber was connected to a volumetric adsorption equipment in order to control amount of adsorption. A10 was ground and packed in a 1mm-thick, slit-shaped cell with beryllium windows.

3. Application of RMC method to adsorption systems

The RMC simulation was carried out so that the difference between an experimental XRD intensity and a simulated intensity should be minimized, different from conventional Monte Carlo (MC) simulation which uses intermolecular potential. Thus, the molecular configuration obtained will be the most consistent with the experimental XRD data.

3.1. X-ray scattering intensity of adsorption systems The adsorption system can be regarded as a 3-phases mixed system comprising adsorbate, solid, and vacant space (void). The experimental XRD intensity of an adsorption system (I_{obs}^{a}) consists of many terms, the self-scattering terms of solid and adsorbed phase and interference terms between admolecules, solid atoms, and admolecules and solid atoms. In addition, a few correction terms such as X-ray absorption due to admolecules were taken into account. The total scattering intensity I_{tot}^{a} may be expressed by the following equation:

$$I_{\mathrm{tot}}^{\mathrm{a}} = \frac{k}{n_{\mathrm{sld}}} P\ G\ A \left\{ I_{\mathrm{sc}}^{\mathrm{s}} + I_{\mathrm{sc}}^{\mathrm{a}} + I_{\mathrm{if}}^{\mathrm{s-s}} + I_{\mathrm{if}}^{\mathrm{a-a}} + I_{\mathrm{if}}^{\mathrm{s-a}} + I_{\mathrm{saxs}} \right\} \quad (1)$$

where k and n_{sld} are the coefficient converting the experimental intensity from e.u.

(electron unit) to c.p.s., and the number of atoms in a solid phase in the simulation cell, respectively. P, G, and A are the correction factors concerning with polarization, X-ray irradiating volume, and X-ray absorption, respectively. I_{sc}^{s} is the scattering term of solid phase, I_{sc}^{a} the scattering term of adsorbed phase, $I_{if}^{s\text{-}s}$ the interference term between solid atoms, $I_{if}^{a\text{-}a}$ between admolecules, $I_{if}^{s\text{-}a}$ between admolecule and solid atom, and I_{saxs} the small angle scattering term. I_{tot}^{a} was simulated and compared with the experimental intensity I_{obs}^{a}.

I_{sc}^{s} and $I_{if}^{s\text{-}s}$ can be obtained from scattering intensity of a porous solid in vacuum, when there are no structural changes of solid phase. I_{sc}^{a}, $I_{if}^{a\text{-}a}$, and $I_{if}^{s\text{-}a}$ can be determined by the simulated molecular configuration of admolecules in the simulation cell. In RMC simulations of liquids and amorphous solids, I_{sc} can be determined by density and molar ratio of the samples. However, in this analysis for adsorption systems, I_{sc} also was simulated, because I_{sc}^{a} and A changed with adsorption amount. We refer to this method as SF-RMC, indicating that the solid phase was fixed through the analysis.

3.2. Models for micropore and admolecule We assumed a pore model for the micropore of A10 in order to estimate $I_{if}^{s\text{-}a}$. The micropore structure was determined from an N_2 adsorption isotherm measured with a gravimetric method at 77 K after pre-heating at 383 K and 1 mPa for 2 h, along with various informations from XRD, magnetic properties, etc [29]. N_2 adsorption isotherm of A10 at 77 K was of Type I. The specific surface area a and the external surface area a^{ext} were determined by the α_s plot [30]. The external surface area was negligibly small compared with a . The micropore volume $W_0(N_2)$ was determined by saturation amount of N_2 adsorption and bulk liquid density (ρ_{N2} = 0.808 g/cm^3). The average pore width w, estimated from a and W_0, was 0.82 nm. The structural parameters of A10 are summarized in Table 1.

We assumed the slit-shaped pore of w = 0.82 nm with graphitic walls comprising double graphene sheets whose interlayer distance Δ was 0.335 nm (Figure 1). w is the effective pore width, different from the distance between centers of carbon atoms at the 1st layer of the wall, H (= $w + \sigma_C$, where σ_C was the diameter of a carbon atom). The size of the simulation cell was set 6.15 × 6.40 nm^2, and the periodic boundary condition was employed. Although the boundary condition corresponds to an infinite model, only the carbons which exist at short distance away from an admolecule contribute to $I_{if}^{s\text{-}a}$, and

thus the model is practically good for the local carbon structure of ACF around an adsorbed C_2H_5OH molecule.

The atomic configuration of a C_2H_5OH molecule was optimized by the AM1 method that was performed with MOPAC [33]. The atomic diameter σ for C, O atom in C_2H_5OH, and C atom in graphene layer were 0.245, 0.218, and 0.340 nm, respectively.

3.3. Scattering and interference terms for solid phase I_{sc}^{s} and $I_{if}^{s\text{-}s}$ were obtained from the scattering intensity I_{obs}^{s} of a porous solid in vacuum:

$$I_{\mathrm{sc}}^{\mathrm{s}} + I_{\mathrm{if}}^{\mathrm{s-s}} = \frac{n_{\mathrm{sld}}}{k} \frac{1}{P\ G\ A} I_{\mathrm{obs}}^{\mathrm{s}} \quad (2)$$

The correction factors and coefficients all are the same as those in eq. 1. The measurements of I_{obs}^{a} and I_{obs}^{s} must be carefully carried out so that the quantity and density of a sample along the X-ray path are kept unchanged. The parasitic scattering which is mainly attributed to the windows of a sample cell is included in both I_{obs}^{a} and I_{obs}^{s}. Therefore, it was removed simultaneously in subtracting the XRD intensity of solid phase I_{obs}^{s}.

3.4. Normalization coefficient of scattering intensity k is determined by fitting the theoretical values in the wide-angle region ($s > 40$ nm^{-1}) to I_{obs}^{s}:

$$\frac{1}{k\ P\ G\ A} I_{\mathrm{obs}}^{\mathrm{s}}(s_{\max}) \simeq \left\{ f_{\mathrm{s}}^{2}(s_{\max}) + \Phi\ i_{\mathrm{s}}^{\mathrm{inc}}(s_{\max}) \right\} \quad (3)$$

where s_{max} is the maximum value of s in the measurement region (the scattering parameter $s = 4\pi \sin\theta/\lambda$, where 2θ is the scattering angle and λ the wave length of an X-ray). The literature values [31] were used for the atomic scattering factor f_s and the incoherent scattering intensity i_s^{inc}. Φ is the ratio of detected intensity to i_s^{inc}, that depends on the experimental condition of monochromatization [32].

3.5. Interference terms The interference terms between admolecules $I_{if}^{a\text{-}a}$ and solid atoms and an admolecule $I_{if}^{s\text{-}a}$ are determined by the following equations:

$$I_{\mathrm{if}}^{\mathrm{a-a}} = \sum_{j_1}^{j_1 \neq j_2} \sum_{j_2} f_{j_1} f_{j_2} \frac{\sin sr_{j_1 j_2}}{sr_{j_1 j_2}} \quad (4)$$

$$I_{\mathrm{if}}^{\mathrm{s-a}} = 2 \sum_{j} \sum_{k} f_j f_k \frac{\sin sr_{jk}}{sr_{jk}} \quad (5)$$

The summation are carried out over all atom pairs of j_1 th and j_2 th admolecules and j th admolecule and k th solid atom in the simulation cell, respectively, except for atom-pairs within a molecule. Here, f is the atomic X-ray scattering factor and r_{jk} is the distance between two positions, j and k. In the case of ACF, eq. 5 may be replaced by eq. 6 after averaged over carbon atoms in graphene walls:

$$I_{\mathrm{if}}^{\mathrm{s-a}} = 2\pi \sum_{j} \sum_{l} f_j f_{\mathrm{C}} \rho_{\mathrm{s}} \frac{\cos sr_{\mathrm{z}}}{s^2} \quad (6)$$

where l denotes l th graphene layer. ρ_s is the atomic density of graphene, 38.1 atom/nm^2, r_z the distance between an atom in admolecule and graphene layer, f_C the atomic scattering factor of carbon.

3.6. Scattering terms The scattering factor of admolecules I_{sc}^{a} includes the following contribution of the interference between atom pairs within a molecule which is not included in eq. 4:

$$I_{\mathrm{sc}}^{\mathrm{a}} = n_{\mathrm{a}} \left\{ \sum_{m}^{N} f_m^2 + \Phi \sum_{m}^{N} i_m^{\mathrm{inc}} + \sum_{m_1}^{m_1 \neq m_2} \sum_{m_2} f_{m_1} f_{m_2} \frac{\sin sr_{m_1 m_2}}{sr_{m_1 m_2}} \right\} \quad (7)$$

where f_m and i_m^{inc} are the atomic scattering factor and incoherent scattering intensity of mth atom in an admolecule ($m \leq N$) and n_a is the number of admolecule in the simulation cell.

Scattering and intra-molecular interference due to an admolecule, i.e., the terms in a bracket of eq. 7, are fixed in the simulation.

3.7. Correction factors The correction factors, P , G, and A, depend on experimental setup. We describe the factors as to the transmission method with an angle-dispersion

diffractometer with a monochrometer. These factors here are partially different from those in previous RDF analysis [6,32].

a. Polarization factor The polarization factor $P(\theta)$ is given by the following equation: [34]

$$P(\theta) = \frac{1 + \cos^2 2\alpha \ \cos^2 2\theta}{1 + \cos^2 2\alpha} \quad (8)$$

where 2α is the scattering angle on the monochrometer.

b. Geometrical factor When the experiment is carried out by a transmission XRD method using a sample having homogeneous thickness, the geometrical factor $G(\theta)$, which normalizes the X-ray irradiating volume, is simplified as the following equation:

$$G(\theta) = \frac{1}{\cos\theta} \quad (9)$$

Practically, this equation was modified using the coefficients c_{geo} and d_{geo} in order to take into account non-ideal shape and orientation of sample particles.

$$G(\theta) = \frac{1}{\cos\theta} \left\{1 + c_{geo} \left(\frac{1}{\cos\theta_{max}} - \frac{1}{\cos\theta}\right)\right\} \left\{1 + d_{geo} \left(\frac{4\pi \sin\theta_{max}}{\lambda} - \frac{4\pi \sin\theta}{\lambda}\right)\right\}$$

(10)

The c_{geo} and d_{geo} were determined by fitting (f_s+ Φ i_s) to I_{obs} in the whole s region using eq. 3.

c. Absorption factor The X-ray absorption factor $A(\theta, n_a/n_{sld})$ is very important in an adsorption system, because the factor depends on not only the scattering angle 2θ but also adsorption amount:

$$A(\theta, \frac{n_a}{n_{sld}}) = \exp\left\{-\left(1 + \frac{n_a}{n_{sld}} \frac{\mu_a}{\mu_s}\right) G(\theta) \ \ln \frac{I^0_{trans}}{I^s_{trans}}\right\} \quad (11)$$

where n_a/n_{sld} is the molar ratio of admolecule to solid atom. I_{trans}^0 and I_{trans}^s are the X-ray intensities transmitted at θ = 0° without and with a sample in vacuum, respectively. Both

I_{trans}^{0} and I_{trans}^{s} were measured at the same tube voltage and current using an aluminum plate of 1 mm thickness as an X-ray attenuator. μ_a and μ_s are the molar X-ray absorption coefficients of admolecule and solid atom, respectively. μ_a can be calculated by the following equation:

$$\mu_{\mathrm{a}} = \sum_{i}^{N} \{(\mu/\rho)_i \; M_i\} \quad (12)$$

where M_i is the atomic mass and $(\mu/\rho)_i$ is the mass X-ray absorption coefficient of atom that is found in literature [31]. The μ_a and μ_s of C_2H_5OH and carbon are 280.19 and 50.67, respectively.

d. Small angle scattering Porous carbons show strong X-ray scattering in the small angle region of $s < 10$ nm^{-1}. I_{saxs} changes greatly with molecular adsorption [35], since large scale information about shape and size of pores [36] and adsorbed molecular assemblies [2,7] are included. I_{saxs} is not the sum of I_{sc} and I_{if} , because the correlation length of the system is larger than the size of molecular assembly and carbon crystallite. We assumed that I_{saxs} should be the following equation:

$$I_{\mathrm{saxs}} = \exp(a_{\mathrm{saxs}} \; \log s + b_{\mathrm{saxs}}) \quad (13)$$

where a_{saxs} and b_{saxs} are the fitting parameter for the experimental SAXS intensity in the small angle region.

3.8. Consistency with experimental amount adsorbed The ratio n_a/n_{sld} in the simulation should agree with the experimental adsorption amount. In this analysis, n_{sld} was determined by combination of the experimental saturation amount of adsorption and density of adsorbate in MC simulation. Assuming that admolecules fill completely pores at the saturation condition,

$$n_{\mathrm{sld}} = \frac{n_{\mathrm{a}}^{\mathrm{max}}}{(m_{\mathrm{a}}/m_{\mathrm{sld}})^{\mathrm{satu}}} \; \frac{M_{\mathrm{a}}}{M_{\mathrm{sld}}} \quad (14)$$

where m_a and m_{sld} are the mass of adsorbate and porous solid, respectively, and $(m_a/m_{sld})^{satu}$ is the experimental saturation amount of adsorption. n^{max}_a is the maximum

number of admolecule in the MC simulation cell at a sufficiently high pressure. Here the simulation cell was kept at the same conditions as the RMC simulation. M_a and M_{sld} are the molecular and atomic mass of admolecule and porous solid, respectively.

3.9. Optimization of molecular configuration in micropore The RMC simulation should be repeated until the experimental diffraction pattern are reproduced exactly using the equations above. New configuration was generated by a trial that was randomly chosen from movement (including rotation), insertion, and deletion of a molecule. In the movement trial, the position of a randomly selected molecule was randomly displaced by a distance of 0.05 nm, then rotated by an angle of 5.7°. The movement trial affects only $I_{if}^{a\text{-}a}$ and $I_{if}^{s\text{-}a}$. In the insertion trial, a new admolecule was generated randomly at a position. In the deletion trial, one of admolecules was randomly deleted. The insertion and deletion trials affect I_{sc}^{a}, $I_{if}^{a\text{-}a}$, $I_{if}^{s\text{-}a}$, and A.

When the distance between an atom in j_1 molecule and an atom in j_2 molecule was less than 0.49 ($\sigma_{j1} + \sigma_{j2}$), the trial was rejected automatically. Other trials were treated according to the usual RMC criteria:

$$\chi^2 = \sum_{s}^{s_{\max}} \frac{\{I_{\mathrm{obs}}^{\mathrm{a}}(s) - I_{\mathrm{tot}}^{\mathrm{a}}(s)\}^2}{\omega^2} \quad (15)$$

$$\Delta\chi^2 = \chi^2_{\mathrm{new}} - \chi^2_{\mathrm{previous}} \quad (16)$$

When the weighed least square difference $\Delta\chi^2$ between simulated and experimental data was negative, the trial was accepted. When $\Delta\chi^2$ was positive, the trial was accepted with a probability of $\exp(-\Delta\chi^2)$. The adopted weighing coefficient ω value was 20 (c.p.s. nm^{-1}), because further decrease in ω led to no improvement in fitting. Any parameter chosen randomly from a_{saxs}, b_{saxs}, and I_{trans}^{s} was changed within 1 % at each trial. The trial was accepted or rejected according to the criteria eqs. 15 and 16. The random number was generated by the Mersenne Twister algorithm [37].

4. Results and Discussion

4.1. C_2H_5OH adsorption The adsorption isotherm of C_2H_5OH on A10 at 300 K is shown in Figure 2. The isotherm is of type I, showing that C_2H_5OH molecules are adsorbed by the micropore filling mechanism. The micropore volume $W_0(C_2H_5OH)$ was determined by saturation amount of C_2H_5OH adsorbed and its bulk liquid density (ρ_{C2H5OH} = 0.787 g/cm^3), as given in Table 1. $W_0(C_2H_5OH)$ was much less than $W_0(N_2)$, i.e., $W_0(C_2H_5OH)/W_0(N_2)$ = 0.73, suggesting serious restriction in packing C_2H_5OH molecules into the micropore.

4.2. XRD profiles of C_2H_5OH adsorbed on ACF Figure 3 shows the experimental XRD profiles of A10 in vacuum (I_{obs}^{s}) and A10 having C_2H_5OH adsorbed at different fractional filling ϕ and 300 K (I_{obs}^{a}). I_{obs}^{s} showed the broad (002) peak at s = 16.9 nm^{-1}. The XRD profile changed with adsorption of C_2H_5OH, and a peak around s = 15.8 nm^{-1} appeared at ϕ = 0.83. The difference between the I_{obs}^{s} and I_{obs}^{a} values is assigned to the interferences both between adsorbed C_2H_5OH molecules and between C_2H_5OH and carbon walls. The sharp peaks at s = 31.7 and 36.2 nm^{-1} are peaks of the beryllium windows. The intensity of these peaks decreased with increasing amount of C_2H_5OH adsorbed because of X-ray absorption due to C_2H_5OH. The intensity of small-angle X-ray scattering (s < 10 nm^{-1}) also decreased with C_2H_5OH adsorption because the density fluctuation of the system decreased with pore filling. Figure 4 shows the corrected XRD profiles of A10 and A10 adsorbing C_2H_5OH, $I_{obs}^{a,corr}$ and $I_{obs}^{s,corr}$ and their difference I_{obs}^{sub}:

$$I_{\mathrm{obs}}^{\mathrm{sub}} = I_{\mathrm{obs}}^{\mathrm{a,corr}} - I_{\mathrm{obs}}^{\mathrm{s,corr}} = \frac{1}{P\ G\ A(\phi)}\ I_{\mathrm{obs}}^{\mathrm{a}} - \frac{1}{P\ G\ A(\phi=0)}\ I_{\mathrm{obs}}^{\mathrm{s}} \tag{17}$$

I_{obs}^{sub} includes the interferences between adsorbed C_2H_5OH molecules and between C_2H_5OH and carbon walls, i.e.,

$$I_{\mathrm{obs}}^{\mathrm{sub}} = \frac{k}{n_{\mathrm{sld}}} \left\{ I_{\mathrm{sc}}^{\mathrm{a}} + I_{\mathrm{if}}^{\mathrm{a-a}} + I_{\mathrm{if}}^{\mathrm{s-a}} \right\} \tag{18}$$

I_{obs}^{sub} was Fourier-transformed into the differential radial distribution functions (RDF) $f_{drdf} \equiv 4\pi r^2(\rho(r) - \rho_0)$). The RDFs of C_2H_5OH adsorbed in micropore and bulk liquid are shown in

Figure 5. The adsorbed C_2H_5OH had greater amplitudes than bulk liquid. The first peak at r = 0.5 nm shifted to a shorter distance compared with that of bulk liquid. Such behavior may arise from immobilization of adsorbed C_2H_5OH except for contribution of $I_{if}^{s\text{-}a}$ to the amplitudes. The structural information of the RDF was transformed to the 3-dimensional structure by the RMC method.

4.3. RMC fits to experimental XRD intensity The RMC simulation was carried out to reproduce the experimental XRD data of C_2H_5OH adsorbed on A10. The calculation was done over 4 million steps, because more calculation did not improve χ^2. Figure 6 shows the experimental scattering intensity (I_{obs}^{a}) at ϕ = 0.83, the RMC simulation curve (I_{tot}^{a}), and the difference (ΔI_r) between I_{obs}^{a} and I_{tot}^{a}. The I_{tot}^{a} fits well the experimental curve.

4.4. Structure of C_2H_5OH assembly in micropore Figure 7 depicts the top- and side-views of the snapshots of molecular configurations of adsorbed C_2H_5OH at ϕ = 0.34 and 0.83. The snapshots contain 98 and 250 C_2H_5OH molecules, respectively. Figure 8 shows the molecular configuration around the upper (z > 0) and lower walls (z < 0). In low fractional filling (ϕ = 0.34), C_2H_5OH molecules covered partially the carbon wall and seemed to form bilayer even at such low coverage, as seen in Figure 9 which shows the weighted average density profiles of carbon and oxygen atoms in C_2H_5OH along the direction perpendicular to the wall surface. It indicates that hydrogen bonds between C_2H_5OH molecules are formed in not only an intra-layer but also inter-layers. In the high fractional filling of ϕ = 0.83, C_2H_5OH also formed bilayer structure in the micropore, and almost uniformly were distributed on the whole surface but not in a closest packing structure (Figure 8). Figure 8 suggest molecular chain structure formed through hydrogen bonds, although the hydrogen bond formation unfortunately was not confirmed by the RMC simulation because no X-ray scattering distinguish clearly oxygen atoms from carbon atoms.

4.5. Comparison with MC simulation The structures of C_2H_5OH adsorbed on A10 were estimated using the canonical Monte Carlo (MC) simulation for comparison. The intermolecular interaction between C_2H_5OH molecules was calculated by the model which was proposed by Stewart et. al., who assumed Lennard-Jones and Coulombic interaction [38] Steele's 10-4-3 potential function [39] was used for the interaction of a C_2H_5OH molecule with a carbon wall. The number of C_2H_5OH adsorbed was set at the

same number as the RMC simulation.

Figure 10 depicts the top- and side-views of the snapshots of the molecular configuration of C_2H_5OH adsorbed at ϕ = 0.34 and 0.83. The red, blue, and green bonds denote the hydrogen bonded oxygen pairs (r < 0.32 nm) in an upper layer (z > 0), a lower layer (z < 0), and between inter-layers. The density profiles of oxygen and carbon atoms obtained from the MC simulation, along with their averaged density, are also shown in Figure 11. The density profiles of RMC configuration is also shown for comparison. The density profiles of RMC configuration agreed well with MC simulation.

Figure 10A shows that C_2H_5OH molecules cover partially the carbon wall at ϕ = 0.34 and form small bilayer structure like the RMC simulation. The number of total hydrogen bond was 103, which corresponded to 2.10 bonds per molecule. The number of inter-layer hydrogen bond (green) was 33, which was 32% of total bond number. Such high fraction of inter-layer hydrogen bond indicates that the hydrogen bond greatly contributes to the bilayer formation of C_2H_5OH adsorbed in this micropore. In Figure 10B, C_2H_5OH molecules form bilayer structure with sparse packing at ϕ = 0.83. The number of total hydrogen bond was 222, which corresponded to 1.78 bonds per molecule. The number of inter-layer hydrogen bond was 80 (36% of total bond number). Since the fraction of inter-layer hydrogen bond was almost equal to the ϕ = 0.34 case, the local structure of C_2H_5OH adsorbed was similar in both cases.

5. Conclusion

The RMC method for structural investigation of an adsorbed phase in micropores was proposed. The method was examined by applying to the wide-angle XRD data of the ACF– C_2H_5OH adsorption system. The RMC simulation fitted the XRD data very well. The simulated results showed that C_2H_5OH molecules form a bilayer structure in the wide region of ϕ in the micropores (w = 0.82 nm). Such molecular configuration agreed well with the result of MC simulation, which also suggests that hydrogen bonds greatly contributes to the bilayer formation in micropores. Thus, the proposed method gave pseudo-3-dimensional structural information of adsorbed phase in micropores. The RMC method would be applied to a model-less adsorbed phase in various adsorption systems, when pore structure such as shape and size is known.

Acknowledgment. This research was supported by the Grant-in-Aid for Young Scientists(A)(No. 19685002) and CLUSTER (the second stage) of Ministry of Education, Culture, Sports, Science and Technology, Japan.

Appendix

Nomenclature

$I_{obs}^{a}(s)$	experimental total XRD intensity of adsorbed system (c.p.s.)
$I_{obs}^{s}(s)$	experimental XRD intensity of porous solid in vacuum (c.p.s.)
I_{trans}^{s}	transmitting XRD intensity of sample in vacuum (c.p.s.)
I_{trans}^{0}	transmitting XRD intensity of no sample (c.p.s.)
$I_{tot}^{a}(s)$	total XRD intensity of adsorbed system by RMC simulation (c.p.s.)
$I_{sc}^{s}(s)$	self-scattering term of solid phase (per unit cell, e.u.)
$I_{sc}^{a}(s)$	self-scattering term of adsorbed phase (per unit cell, e.u.)
$I_{if}^{s-s}(s)$	interference term between solid atoms (per unit cell, e.u.)
$I_{if}^{a-a}(s)$	interference term between admolecules (per unit cell, e.u.)
$I_{if}^{s-a}(s)$	interference term between admolecule-solid atom (per unit cell, e.u.)
$I_{saxs}(s)$	small angle scattering (per unit cell, e.u.)
n_a	number of admolecule in the unit cell
n^{max}_a	maximum number of admolecule in the unit cell
n_{sld}	number of solid atoms corresponded with unit cell
k	intensity converting coefficient from e.u. to c.p.s.
$f(s)$	atomic/molecular scattering factor (per atom/molecule, e.u.)
μ	molar X-ray absorption coefficient
(μ/ρ)	mass X-ray absorption coefficient (cm^2/g)
$i^{inc}(s)$	incoherent scattering (per atom, e.u.)
a_{saxs}, b_{saxs}	correcting coefficients for the small angle scattering
c_{geo}, d_{geo}	correcting coefficients for the X-ray irradiating volume
ϕ	fractional filling of adsorbate in the pore

s	scattering parameter ($s = 4\pi \sin\theta/\lambda$, nm^{-1})
w	effective pore width (nm)
r_{j1j2}	atomic distance between admolecules (nm)
r_{jk}	atomic distance between admolecule and carbon atom (nm)
r_{m1m2}	atomic distance of intramolecule (nm)
r_z	atomic distance from the graphene layer (nm)
σ	atomic diameter (nm)
$\Delta\chi^2$	weighed least square difference between the $I_{obs}{}^a$ and $I_{tot}{}^a$
ω	weighing coefficient in the simulation

(e.u. = electron unit, c.p.s. = count per second

References

[1] D. H. Everett, J. C. Powl, J. Chem. Soc., Faraday Trans. 72 (1976) 619.

[2] T. Iiyama, Y. Kobayashi, K. Kaneko, S. Ozeki, Coll. Surf. A 241 (2004) 207.

[3] T. Iiyama, K. Nishikawa, T. Otowa, K. Kaneko, J. Phys. Chem. 99 (1995) 10075.

[4] T. Iiyama, K. Nishikawa, T. Suzuki, K. Kaneko, Chem. Phys. Lett. 274 (1997) 152.

[5] T. Iiyama, T. Suzuki, K. Kaneko, Chem. Phys. Lett. 259 (1996) 37.

[6] T. Iiyama, K. Nishikawa, T. Suzuki, T. Otowa, M. Hijiriyama, Y. Nojima, K. Kaneko, J. Phys. Chem. B 101 (1997) 3037.

[7] T. Iiyama, M. Ruike, K. Kaneko, Chem. Phys. Lett. 331 (2000) 359.

[8] T. Ohba, H. Kanoh, K. Kaneko, J. Am. Chem. Soc. 126 (2004) 1560.

[9] S. Takamizawa, E. Nakata, T. Saito, K. Kojima, CrystEngComm 5 (2003) 411.

[10] S. Horike, R. Matsuda, R. Kitaura, S. Kitagawa, T. Iijima, K. Endo, Y. Kubota, M. Takata, Chem. Commun. (2004) 2152.

[11] T. Ohkubo, T. Konishi, Y. Hattori, H. Kanoh, T. Fujikawa, K. Kaneko, J. Am. Chem. Soc. 124 (2002) 11860.

[12] A. V. Vernov, W. A. Steele, J. Phys. Chem. 97 (1993) 7660.

[13] R. F. Cracknell, K. E. Gubbins, M. Maddox, D. Nicholson, Acc. Chem. Res. 28 (1995) 281.

[14] N. A. Seaton, J. P. R. B. Walton, N. Quirke, Carbon 27 (1989) 855.

[15] T. Suzuki, T. Iiyama, K. E. Gubbins, K. Kaneko, Langmuir 15 (1999) 5870.

[16] S. K. Bhatia, K. Tran, T. X. Nguyen, D. Nicholson, Langmuir 20 (2004) 9612.

[17] K. Koga, X. C. Zeng, H. Tanaka, Phys. Rev. Lett. 79 (1997) 5013.

[18] C. L. McCallum, T. J. Bandosz, S. C. McGrother, E. A. M¨uller, K. E. Gubbins, Langmuir 15 (1999) 533.

[19] G. Hummer, J. C. Rasaiah, J. P. Noworyta, Nature 414 (2001) 188.

[20] A. A. Chialvo, J. Chem. Phys. 92 (1990) 673.

[21] S. Gavalda, K. E. Gubbins, Y. Hanzawa, K. Kaneko, K. T. Thomson, Langmuir 18 (2002) 2141.

[22] J. Pikunic, R. J. -M. Pellenq, K. T. Thomson, J. -N. Rouzaud, P. Levitz, K. E. Gubbins, Studies in Surface Science and Catalysis Vol. 132 Elsevier, Amsterdam, 2001, 647.

[23] I. Bak´o, P. Jedlovszky, G. P´alink´as, J. Mol. Liquids 87 (2000) 243.

[24] L. Pusztai, R. L. McGreevy, Mol. Phys. 90 (1997) 533.

[25] M. Misawa, J. Chem. Phys. 116 (2002) 8463.

[26] K. Morishige, J. Chem. Phys. 97 (1992) 2084.

[27] T. Ohkubo, T. Iiyama, K. Nishikawa, T. Suzuki, K. Kaneko, J. Phys. Chem. B 103 (1999) 1859.

[28] T. Iiyama, R. Aragaki, T. Urushibara, S. Ozeki, Adsorp. Sci. Technol. 24 (2006) 815.

[29] K. Kaneko, K. Yamaguchi, C. Ishii, S. Ozeki, S. Hagiwara, T. Suzuki, Chem. Phys. Lett. 176 (1991) 75.

[30] K. Kaneko, C. Ishii, M. Ruike, H. Kuwabara, Carbon 30 (1992) 1075.

[31] C. H. MacGillavry, International Tables for X-ray Crystallography Vol. IV, Kluwer Aca-demic Publishers, Dordrecht, 1989.

[32] T. Iiyama, T. Ohkubo, K. Kaneko, Recent Advances in Gas Separation by Ceramic Membranes, Elsevier, Amsterdam, 2000, 35.

[33] J. J. P. Stewart, QCPE Bull. 9 (1989) 10.

[34] A. Guinier, X-ray Diffraction In Crystals, Imperfect Crystals, and Amorphous Bodies, W. H. Freeman and Company, San Francisco, 1963.

[35] Y. Fujiwara, K. Nishikawa, T. Iijima, K. Kaneko, J. Chem. Soc., Faraday Trans. 87 (1991) 2763.

[36] M. Ruike, T. Kasu, N. Setoyama, T. Suzuki, K. Kaneko, J. Phys. Chem. 98 (1995) 9594.

[37] M. Matsumoto, T. Nishimura, ACM Trans. Model. Comput. Simul. 8 (1998) 3.

[38] E. Stewart, R. L. Shields, R. S. Taylor, J. Phys. Chem. B 107 (1996) 2333.

[39] W. A. Steele, Surf. Sci. 36 (1973) 317.

TABLE 1: Characteristics of A10. Micropore volume, W_0; total surface area, a ; external surface area, a^{ext}; average pore width, w.

	$W_0(N_2)$ / ml·g^{-1}	$W_0(C_2H_5OH)$ / ml·g^{-1}	a / m^2·g^{-1}	a^{ext} / m^2·g^{-1}	w / nm
A10	0.66	0.48	1510	25	0.82

TABLE 2: Parameters of C_2H_5OH adsorbed in a micropore (0.82 nm) of an activated carbon fiber A10 at 300 K, which were used in RMC simulation

parameters	final values
k	91
n_{sld}	3818
c_{geo}	0.282
d_{geo}	0.604
$\log(I_{trans}^{S}/I_{trans}^{U})$	-0.76

Figure Captions

Figure 1. Schematic illustration of the simulation cell, whose wall is comprised a double graphene sheet.

Figure 2. Adsorption isotherm of C_2H_5OH on A10 at 300 K.

Figure 3. X-ray scattering intensities of A10 adsorbing C_2H_5OH at 300 K. Broken line, A10 in vacuum (I_{obs}^{s}); thin solid line, C_2H_5OH adsorbed on A10 (I_{obs}^{a}, ϕ = 0.34); bold solid line, C_2H_5OH adsorbed on A10 (ϕ = 0.83).

Figure 4. Corrected X-ray scattering intensities of A10 adsorbing C_2H_5OH at 300 K. Broken line, A10 itself; thin solid line, C_2H_5OH adsorbed on A10 (ϕ = 0.83). bold solid line, adsorbed C_2H_5OH.

Figure 5. Dfferential radial distribution functions of adsorbed C_2H_5OH in a micropore (0.82 nm) of A10 at 300 K. Broken line, bulk liquid C_2H_5OH; thin solid line, adsorbed C_2H_5OH (ϕ = 0.34); bold solid line, adsorbed C_2H_5OH (ϕ = 0.83).

Figure 6. A. Experimental XRD intensities of A10 adsorbing C_2H_5OH (I_{obs}^{a}) and RMC simulation of A10 adsorbing C_2H_5OH (I_{tot}^{a}). Broken line, I_{obs}^{a}; solid line, I_{tot}^{a}. B. The difference between the experimental and RMC curves, $I_{obs}^{a} - I_{tot}^{a}$.

Figure 7. Snapshots of layer structure of C_2H_5OH adsorbed in a micropore (0.82 nm) of A10 at 300 K by RMC simulation. A. ϕ = 0.34; B. ϕ = 0.83.

Figure 8. Snapshots of layer structure of C_2H_5OH adsorbed in a micropore (0.82 nm) of A10 at 300 K by RMC simulation. A and B, ϕ = 0.34; C and D, at ϕ = 0.83. A and C, upper layer ($z > 0$); B and D, lower layer ($z < 0$).

Figure 9. Density profiles of adsorbed C_2H_5OH along the direction perpendicular to the surface (along z-axis) by RMC simulation. Thin solid line, ϕ = 0.34; bold solid line, ϕ = 0.83.

Figure 10. MC simulated snapshots of C_2H_5OH adsorbed in a micropore (0.82 nm) of A10 at 300 K. Black, red, and blue spheres are carbon atom, oxygen atom at upper layer ($z > 0$), and oxygen atom at lower layer ($z < 0$), respectively. Bonds denote the hydrogen bonded oxygen pairs ($r < 0.32$ nm): Red, blue, and green bonds are upper intra-layer, lower intra-layer, and inter-layers, respectively. A. ϕ = 0.34; B. ϕ = 0.83.

Figure 11. Density profiles of adsorbed C_2H_5OH along the direction perpendicular to the surface (along z-axis). Thin solid black line, from RMC simulation (ϕ = 0.34); thin broken red line, from MC simulation (weighted average of oxygen and carbon, ϕ = 0.34); bold solid black line, RMC (ϕ = 0.83); bold broken red line, MC (ϕ = 0.83).

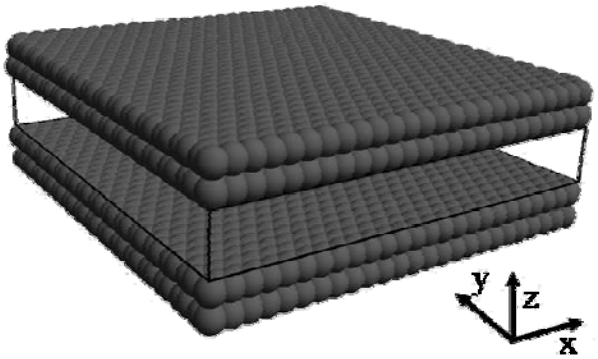

Figure 1. Schematic illustration of the simulation cell, whose wall is comprised a double graphene sheet.

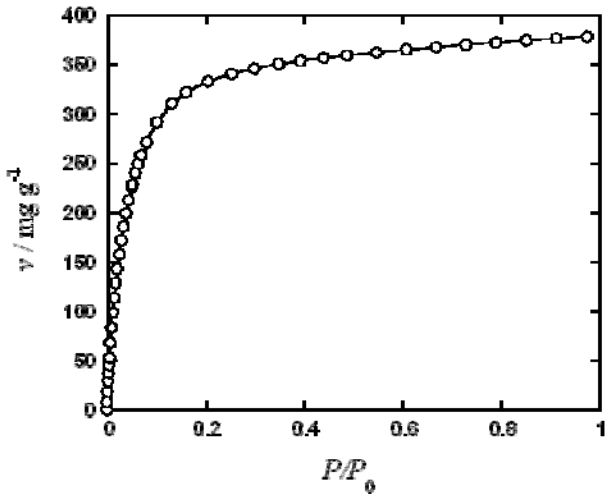

Figure 2. Adsorption isotherm of C_2H_5OH on A10 at 300 K.

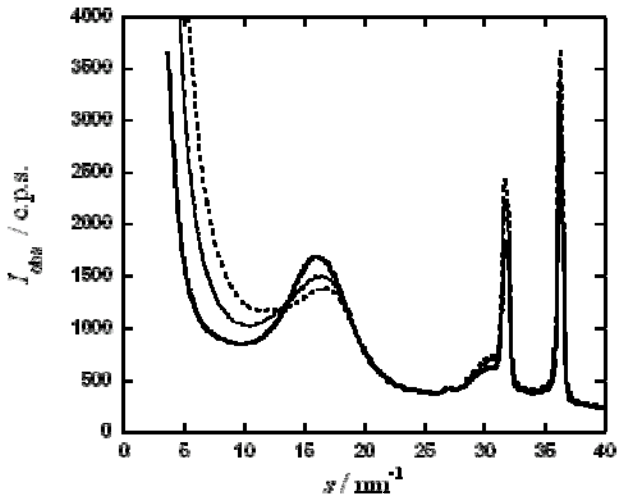

Figure 3. X-ray scattering intensities of A10 adsorbing C_2H_5OH at 300 K. Broken line, A10 in vacuum (I_{obs}^{s}); thin solid line, C_2H_5OH adsorbed on A10 (I_{obs}^{a}, ϕ = 0.34); bold solid line, C_2H_5OH adsorbed on A10 (ϕ = 0.83).

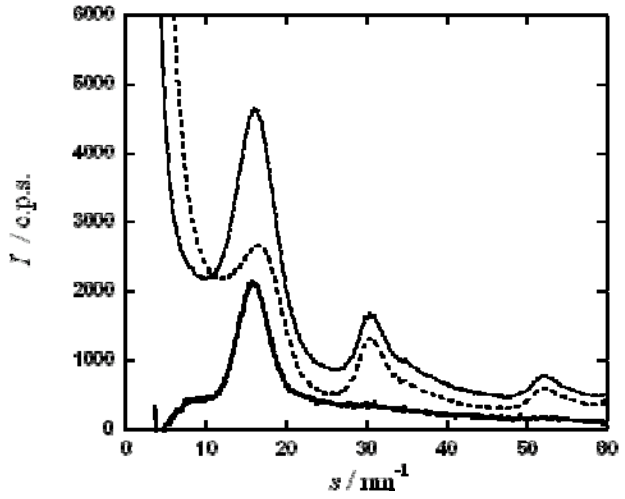

Figure 4. Corrected X-ray scattering intensities of A10 adsorbing C_2H_5OH at 300 K. Broken line, A10 itself; thin solid line, C_2H_5OH adsorbed on A10 (ϕ = 0.83). bold solid line, adsorbed C_2H_5OH.

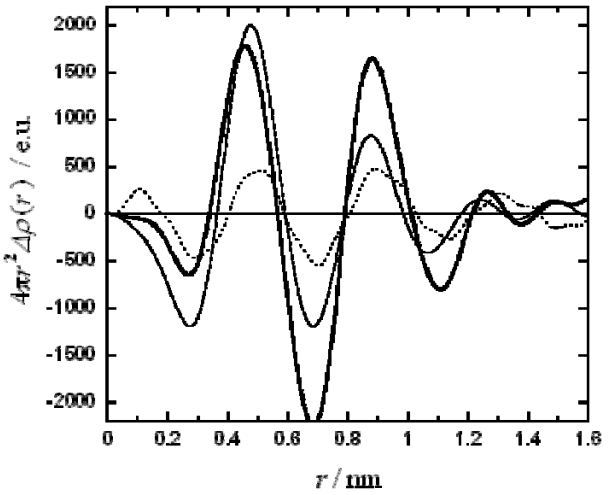

Figure 5. Differential radial distribution functions of adsorbed C_2H_5OH in a micropore (0.82 nm) of A10 at 300 K. Broken line, bulk liquid C_2H_5OH; thin solid line, adsorbed C_2H_5OH (ϕ = 0.34); bold solid line, adsorbed C_2H_5OH (ϕ = 0.83).

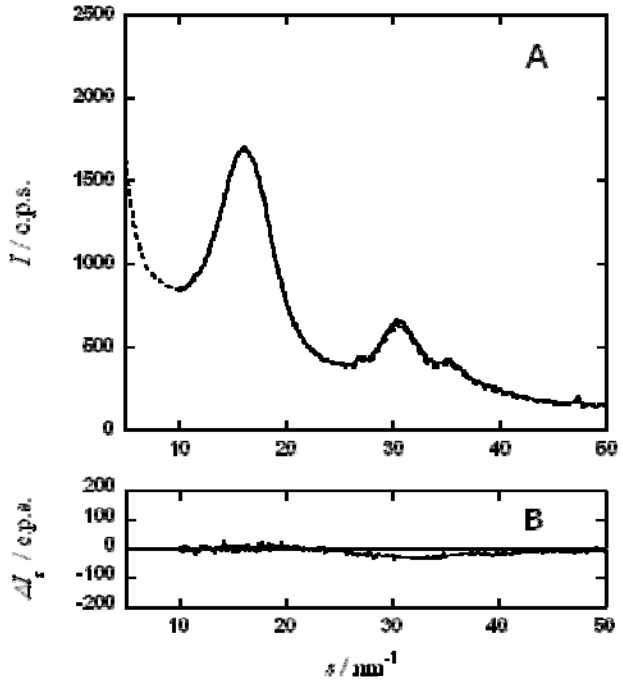

Figure 6. A. Experimental XRD intensities of A10 adsorbing C_2H_5OH (I_{obs}^{a}) and RMC simulation of A10 adsorbing C_2H_5OH (I_{tot}^{a}). Broken line, I_{obs}^{a}; solid line, I_{tot}^{a}. B. The difference between the experimental and RMC curves, $I_{obs}^{a} - I_{tot}^{a}$.

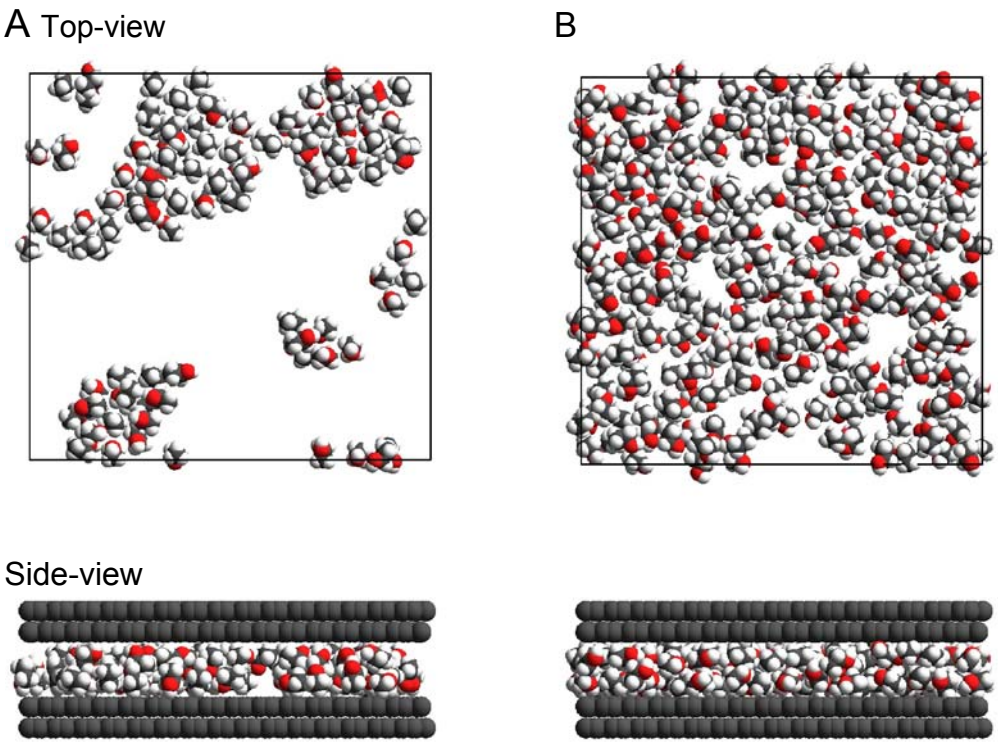

Figure 7. Snapshots of layer structure of C_2H_5OH adsorbed in a micropore (0.82 nm) of A10 at 300 K by RMC simulation. A. ϕ = 0.34; B. ϕ = 0.83.

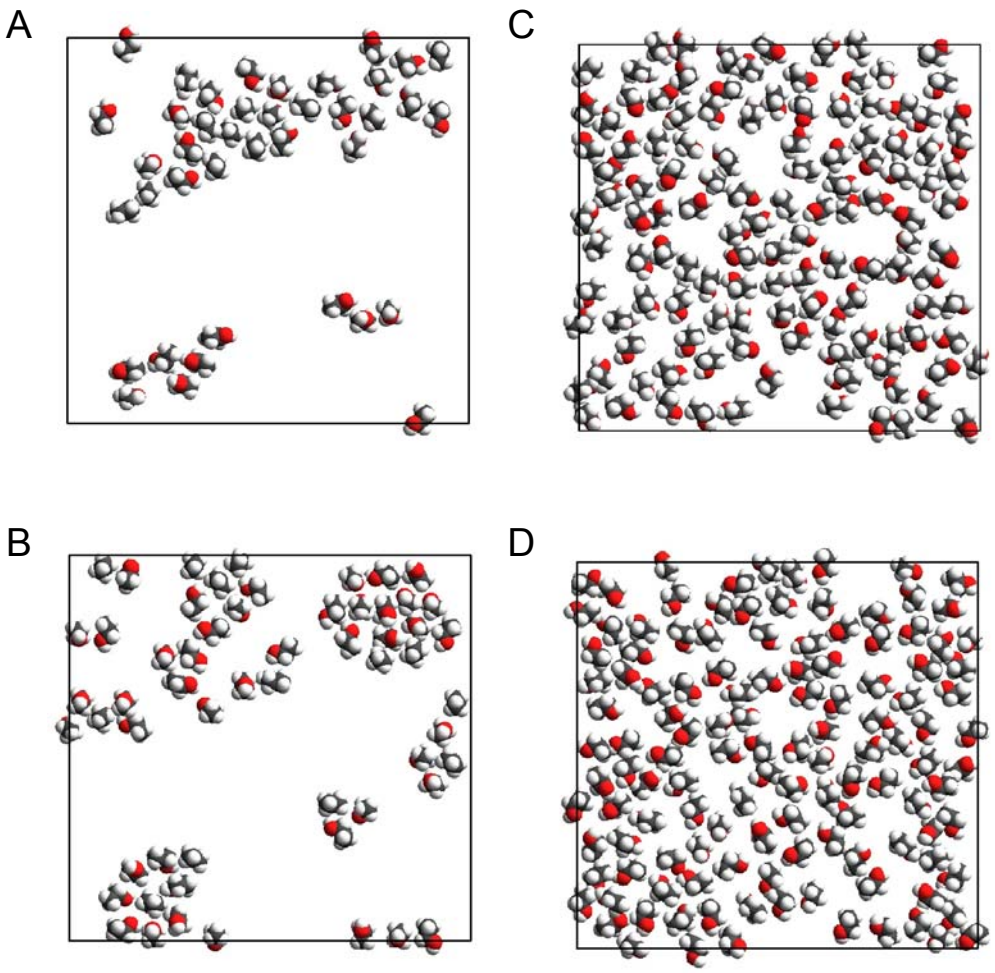

Figure 8. Snapshots of layer structure of C_2H_5OH adsorbed in a micropore (0.82 nm) of A10 at 300 K by RMC simulation. A and B, ϕ = 0.34; C and D, at ϕ = 0.83. A and C, upper layer ($z > 0$); B and D, lower layer ($z < 0$).

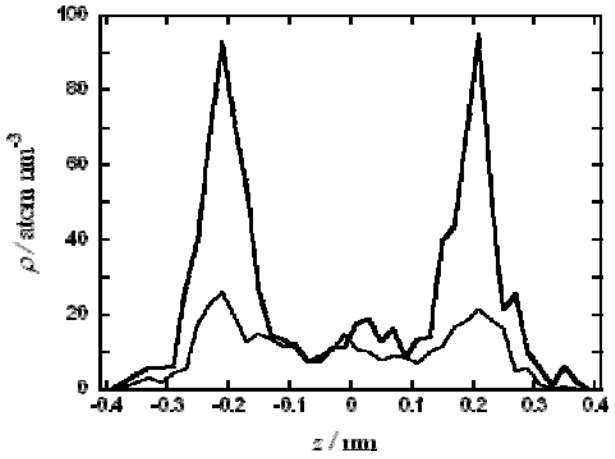

Figure 9. Density profiles of adsorbed C_2H_5OH along the direction perpendicular to the surface (along z-axis) by RMC simulation. Thin solid line, ϕ = 0.34; bold solid line, ϕ = 0.83.

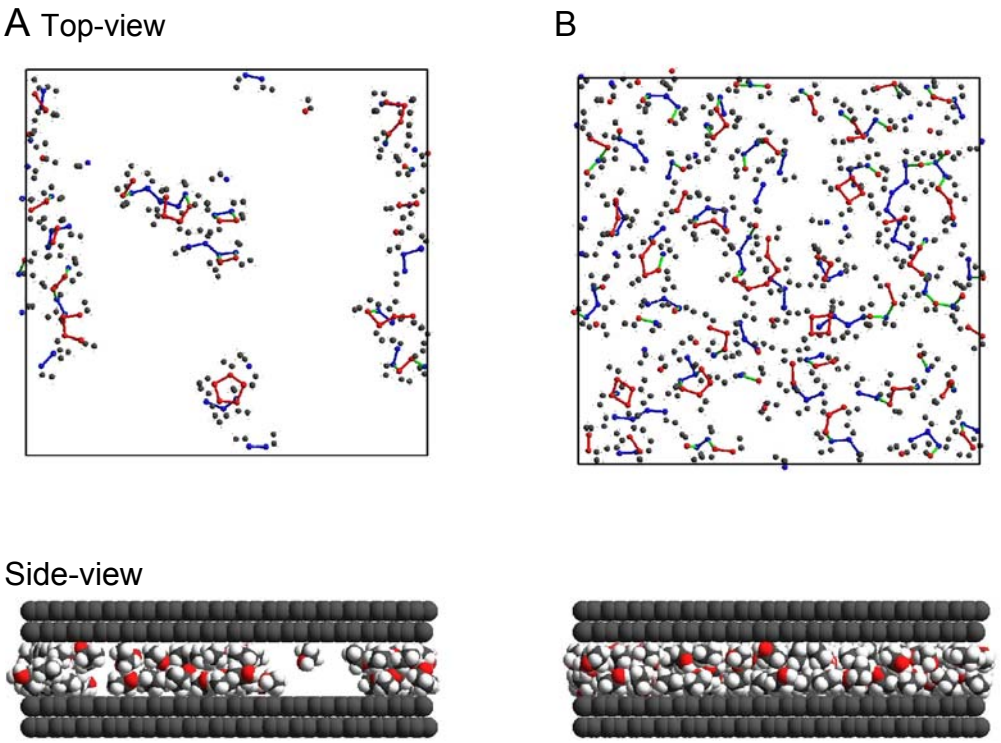

Figure 10. MC simulated snapshots of C_2H_5OH adsorbed in a micropore (0.82 nm) of A10 at 300 K. Black, red, and blue spheres are carbon atom, oxygen atom at upper layer ($z > 0$), and oxygen atom at lower layer ($z < 0$), respectively. Bonds denote the hydrogen bonded oxygen pairs ($r < 0.32$ nm): Red, blue, and green bonds are upper intra-layer, lower intra-layer, and inter-layers, respectively. A. ϕ = 0.34; B. ϕ = 0.83.

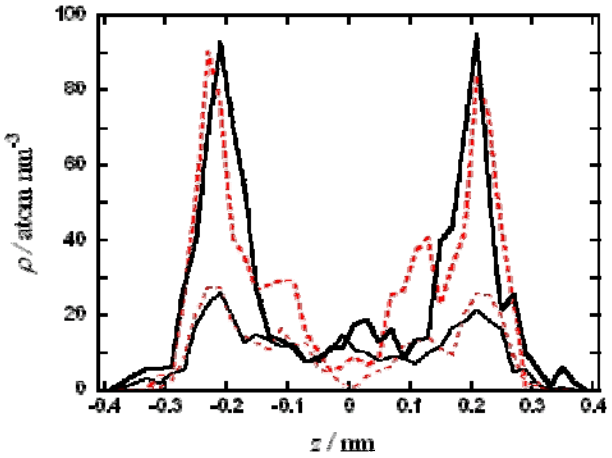

Figure 11. Density profiles of adsorbed C_2H_5OH along the direction perpendicular to the surface (along z-axis). Thin solid black line, from RMC simulation (ϕ = 0.34); thin broken red line, from MC simulation (weighted average of oxygen and carbon, ϕ = 0.34); bold solid black line, RMC (ϕ = 0.83); bold broken red line, MC (ϕ = 0.83).